Journal for ImmunoTherapy of Cancer

Blockade of glucose-6-phosphate dehydrogenase induces immunogenic cell death and accelerates immunotherapy

Motoki Nakamura ,[1] Tetsuya Magara,[1] Maki Yoshimitsu,[1] Shinji Kano,[1] Hiroshi Kato,[1] Keisuke Yokota,[2] Katsuhiro Okuda,[2] Akimichi Morita[1]

To cite: Nakamura M, Magara T, Yoshimitsu M, *et al*. Blockade of glucose-6-phosphate dehydrogenase induces immunogenic cell death and accelerates immunotherapy. *Journal for ImmunoTherapy of Cancer* 2024;**12**:e008441. doi:10.1136/jitc-2023-008441

Accepted 07 July 2024

[1]Department of Geriatric and Environmental Dermatology, Nagoya City University Graduate School of Medical Sciences and Medical School, Nagoya, Japan
[2]Department of Oncology, Immunology and Surgery, Nagoya City University Graduate School of Medical Sciences, Nagoya, Japan

Correspondence to
Dr Motoki Nakamura;
motoki1@med.nagoya-cu.ac.jp

ABSTRACT

Background Enhanced glucose metabolism has been reported in many cancers. Glucose-6-phosphate dehydrogenase (G6PD) is a rate-limiting enzyme involved in the pentose phosphate pathway, which maintains NADPH levels and protects cells from oxidative damage. We recently found that low G6PD expression correlates with active tumor immunity. However, the mechanism involving G6PD and tumor immunity remained unclear.

Methods We conducted in vitro studies using G6PD-knocked down malignant melanoma cells, pathway analysis using the GEO dataset, in vivo studies in combination with immune checkpoint inhibitors (ICIs) using a mouse melanoma model, and prognostic analysis in 42 melanoma patients and 30 lung cancer patients who were treated with ICIs.

Results Inhibition of G6PD, both chemically and genetically, has been shown to decrease the production of NADPH and reduce their oxidative stress tolerance. This leads to cell death, which is accompanied by the release of high mobility group box 1 and the translocation of calreticulin to the plasma membrane. These findings suggested that inhibiting G6PD can induce immunogenic cell death. In experiments with C57BL/6 mice transplanted with G6PD-knockdown B16 melanoma cells and treated with anti-PD-L1 antibody, a significant reduction in tumor size was observed. Interestingly, inhibiting G6PD in only a part of the lesions increased the sensitivity of other lesions to ICI. Additionally, out of 42 melanoma patients and 30 lung cancer patients treated with ICIs, those with low G6PD expression had a better prognosis than those with high G6PD expression (p=0.0473; melanoma, p=0.0287; lung cancer).

Conclusion G6PD inhibition is a potent therapeutic strategy that triggers immunogenic cell death in tumors, significantly augmenting the efficacy of immunotherapies.

WHAT IS ALREADY KNOWN ON THIS TOPIC

⇒ Enhanced glucose metabolism including pentose phosphate pathway in tumors is known and inhibition of glucose-6-phosphate dehydrogenase (G6PD) as a strategy in cancer therapy is tried. In our previous reports, low G6PD expression correlates with activated tumor immunity. However, the mechanism involving G6PD and tumor immunity remained unclear.

WHAT THIS STUDY ADDS

⇒ This study reveals a mechanism linking G6PD and tumor immunity: G6PD protects cancer cells from immunogenic cell death (ICD), and induction of ICD by G6PD inhibition is a novel therapeutic strategy.

HOW THIS STUDY MIGHT AFFECT RESEARCH, PRACTICE OR POLICY

⇒ Although G6PD inhibition alone has so far failed to lead to practical application, this study shows that the combination of G6PD inhibition and immunotherapy is promising. This will encourage plans for clinical trials.

INTRODUCTION

Our recent studies in Merkel cell carcinoma revealed that the intensity of glucose-6-phosphate dehydrogenase (G6PD) expression is an indicator of tumor typing based on immune activity and inversely correlates with programmed death ligand-1 (PD-L1) expression in tumor cells and prognosis.[1] G6PD expression in tumors and G6PD activity in serum were suggested to be useful biomarkers in immunotherapy. However, how G6PD relates to tumor immunity and immunotherapy, including immune checkpoint inhibitors (ICIs), remains unclear.

G6PD is the rate-limiting enzyme of pentose phosphate pathway (PPP), catalyzing the first step in the oxidative process of PPP, in which decarboxylation produces pentoses such as deoxyribose and ribose, which are necessary for nucleic acid synthesis, and 2 moles of NADP+ (nicotinamide adenine dinucleotide phosphate) are reduced to NADPH. Deoxyribose and ribose are the raw materials for nucleic acid synthesis, and NADPH is used as an antioxidant to remove reactive oxygen species.[2] The role of G6PD in cells is well understood by its deficiency. G6PD

deficiency is an X-linked genetic enzyme deficiency that occurs predominantly in African Americans. When G6PD deficiency prevents the production of NADPH at PPP, red blood cells, which lack mitochondria and use PPP as their sole source of NADPH, become particularly vulnerable to oxidative stress. This leads to hemolytic anemia after acute illnesses such as fevers, and viral or bacterial infections that increase oxidative stress, or after ingestion of oxidizing drugs such as salicylic acid or sulfonamides.[3] NADPH exerts its antioxidant stress effects on cells other than erythrocytes, and cells with high G6PD expression are thought to accumulate less oxidative stress and undergo less cellular senescence.

G6PD is present in the cytoplasm of all cells, but its expression is higher in cancer cells than in normal cells. This is because proliferating cells require more ribose-5-phosphate, a product of PPP, for nucleic acid synthesis. In addition, NADPH, a by-product of PPP, contributes to the antioxidant resistance of tumor cells. The hypermetabolism of cancer cells in the glycolytic pathway, including PPP, is referred to as the "Warburg effect".[4] Since cancer cells produce ATP in the glycolytic pathway even under aerobic conditions, their choice of inefficient glycolytic ATP production over efficient mitochondrial oxidative phosphorylation may be due not only to adaptation to hypoxic conditions but also to the supply of nucleic acids and NADPH.[5–7] This enhanced glucose metabolism in tumors has also been applied to positron emission tomography using fluorodeoxyglucose.

Low G6PD activity causes premature cell senescence and cell death due to oxidative stress while aberrant activation of G6PD causes uncontrolled cell growth and differentiation.[8] Elevated G6PD activity upregulates antiapoptotic factors and inhibits cell cycle proteins.[9] Increased G6PD activity and PPP activation are observed in the G1 and late S phase of the cell cycle and are closely related to DNA synthesis and replication in cancer cells.[10] Elevated G6PD activity also promotes epithelial transformation of cancers[11] and enhances vascular endothelial cell proliferation, migration, and angiogenesis by stimulating endothelial NO synthase activity and carbon monoxide production by vascular endothelial cells.[12 13] Overexpression of G6PD enhances stress tolerance of cancer cells, which is closely associated with resistance to chemotherapy and radiotherapy.[14 15] G6PD has been reported to be associated with cisplatin resistance in non-small cell lung cancer,[16] erlotinib resistance in pancreatic cancer,[17] and doxorubicin resistance in colon cancer.[18] Thus, G6PD activity has been reported to be a biomarker as a prognostic factor in various cancers,[19–21] but no one has described the mechanism of its association with tumor immunity. We hypothesized that inhibition of G6PD induces immunogenic cell death (ICD), which is cell death accompanied by antigen presentation.

MATERIALS AND METHODS

Cell culture

Human melanoma cell lines, SK-Mel-28 (ATCC, Manassas, Virginia, USA) and COLO679 (Riken, Tokyo, Japan) were cultured in RPMI 1640 culture medium (Gibco, Life Technologies, Carlsbad, California, USA) with 10% fetal bovine serum (FBS). Human melanoma cell line A375 (ECACC, Salisbury, UK) was cultured in Dulbecco's modified eagle medium (DMEM, Gibco) with 15% FBS. Mouse melanoma cell line B16 (Riken) was cultured in DMEM with 10% FBS.

Inhibition of G6PD

Chemical inhibition of G6PD was performed by the addition of G6PDi-1 (Cayman Chemical, Ann Arbor, Michigan, USA) for 24 hours. Genetic blocking of G6PD was performed using shRNA plasmid (sc-60667-SH, Santa Cruz Biotechnology, Santa Cruz, California, USA). Transfection was performed according to the protocol provided by the supplier. Control shRNA plasmid (sc-108060, Santa Cruz) was used as a negative control. The transfected cells were cultured in a medium with puromycin. Real-time PCR and high mobility group box 1 (HMGB1) assay were also performed by different three shRNA sequences for G6PD (abx-951683, Abbexa, Cambridge, UK) and control shRNA plasmid (abx-991273, Abbexa) with similar results.

Real-time PCR

messenger RNA (mRNA) purification was performed using an RNeasy Mini kit (Qiagen, Hilden, Germany). The mRNA was converted to cDNA using a High-Capacity cDNA Reverse Transcription Kit (Applied Biosystems, Foster City, California, USA) and PT-100 Programmable Thermal Controller (MJ Research, Watertown, Massachusetts, USA). Real-time PCR was run in triplicate on a DNA Engine Opticon 2 system (MJ Research) using Platinum SYBR Green qPCR Supermix UDG (Invitrogen, Carlsbad, California, USA) and the oligonucleotide primers (Eurofins Genomics, Tokyo, Japan). The levels of gene expression were relative to β-actin expression. The gene-specific forward and reverse primers sequences used were as follows: G6PD, 5'-CTGTTCCGTGAGGACCAGATCT-3' (forward) and 5'-TGAAGGTGAGGATAACGCAGGC-3' (reverse); β-actin, 5'-CCCCAGGCACCAGGGCGTGAT-3' (forward) and 5'-GGTCATCTTCTCGAGGTTGGCCTT GGGGT-3' (reverse).

XTT assay

2,3-Bis-(2-Methoxy-4-Nitro-5-Sulfophenyl)-2H-Tetrazolium-5-Carboxanilide (XTT) assay was performed by using Cell Proliferation Kit II (Roche, Basel, Switzerland). Cells were treated with various concentrations of hydrogen peroxide (H_2O_2) for 24 hours, then labeled according to protocols provided by the supplier, and absorbance was measured at 492 and 690 nm using SPECTRAmax 340PC Microplate Spectrophotometer (Molecular Devices, Sunnyvale, California, USA).

NADP+/NADPH assay

NADP/NADPH Assay Kit-WST (Dojindo, Kumamoto, Japan) was used for the assay. The assay was performed according to protocols provided by the supplier. COLO679 human melanoma cells were used for chemical inhibition by G6PDi-1 and A375 human melanoma cells and B16 mouse melanoma cells for genetic blockade by shRNA plasmid.

HMGB1 assay

HMGB1 ELISA Kit Exp (Shino-Test, Tokyo, Japan) was used for the assay. The assay was performed according to protocols provided by the supplier. COLO679 melanoma cells were used for chemical inhibition by G6PDi-1 and A375 melanoma cells for genetic blockade by shRNA plasmid.

Immunocytochemistry

COLO679 melanoma cells treated with 200 µM H_2O_2 for 2 hours in eight-well chamber slides (Nunc, Roskilde, Denmark) were processed for indirect immunofluorescence to detect the expression of signal transduction proteins using primary antibodies to Anti-Calreticulin (1:75, ab2907, Abcam, Cambridge, UK) and Anti-β-actin (1:620, ab6276-100, Abcam). Bound antibodies were visualized with appropriate secondary antibodies, Alexa Fluor 594 goat anti-Rabbit IgG (Invitrogen) and Alexa Flour 488 goat anti-Mouse IgG (Invitrogen) at 37°C for 30 min at 1:500 dilution with 5% goat serum. 4′,6-Diamidino-2-phenylindol, dihydrochloride (DAPI, Vector Laboratories, Burlingame, California, USA) was used as a counterstain. The fluorescence of red produced by Alexa 594, green by Alexa 488, and blue by DAPI was observed and captured using a fluorescence microscope BZ-X810 (Keyence, Osaka, Japan).

Clustering and gene set enrichment analysis

The in silico analyses were performed using the profiled data set containing 83 melanoma samples containing 31 primary and 52 metastatic lesions with comprehensive gene expression analysis for 13,488 genes accessible at GEO database (GSE8401).[22] A clustered heatmap of all samples was generated using the online tool iDEP.96 (http://bioinfomatics.sdstate.edu/idep/).[23] The same tool was used for generally applicable gene-set enrichment (GAGE) analysis, GO (gene ontology) biological process was selected for gene sets and pathway significance cut-off (false discovery rate; FDR) was set to 0.2.

Melanoma mouse models

All animal experiments conducted were approved by the university's ethics committee (No. 21-024H03). 1×10^7 B16 melanoma cells knocked down G6PD using shRNA plasmid (Santa Cruz) were injected subcutaneously into the back of 6-week-old C57BL/6 female mice. Mice injected in the back with B16 melanoma cells transfected with the empty vector using Control shRNA Plasmid-A as described above were used as controls. 6 days later, twice-weekly 200 µg/mouse anti-PD-L1 antibody (Leinco Technologies, St. Louis, Missouri, USA) or phosphate-buffered saline (PBS) intraperitoneally injections started. After a total of five PD-L1 or PBS injections, the mice were sacrificed 23 days after tumor injection. Tumor volume was measured with calipers and the number of infiltrating lymphocytes with immunohistochemistry. Each group consisted of five mice and all experiments were performed in triplicate as the smallest number that can be statistically analyzed. If some mice died during the course of the experiment, all tumor size measurements for those mice were excluded.

Immunohistochemistry

Undyed formalin-fixed paraffin-embedded (FFPE) tissue slides (Nunc) were processed for indirect immunofluorescence to detect the expression of signal transduction proteins using primary antibodies to the anti-CD8 antibody (1:500, ab217344, Abcam, 1:100, #14-0195-82, Invitrogen) and anti-PD1 antibody (1:500, ab214421, Abcam). Bound antibodies were visualized with the appropriate secondary antibodies, Alexa Fluor 594 goat anti-rabbit IgG (Invitrogen), Alexa Flour 594 goat anti-rat IgG (Invitrogen) and Alexa Flour 488 goat anti-rabbit IgG (Invitrogen) at 37°C for 30 min at 1:500 dilution with 5% goat serum. DAPI (Vector Laboratories) was used as a counterstain. The red fluorescence produced by Alexa 594 and blue fluorescence produced by 4′,6-diamidino-2-phenylindol were observed and captured using a fluorescence microscope BZ-X810 (Keyence). After evaluating entire specimens, CD8-positive cells were counted in 3–5 locations with a high density of infiltrating cells, and the mean value was calculated.

Cohort studies

All patients who received ICI treatment at Nagoya City University between July 2014 and March 2021 for malignant melanoma and between January 2016 and March 2022 for lung cancer, had an FFPE sample stored and were followed for at least 6 months were collected. 42 melanoma patients and 30 lung cancer patients were included. The melanoma cohort included 26 men and 16 women with a median age of 70. The lung cancer cohort consisted of 26 males and 4 females, with a mean age of 68.8. FFPE samples obtained from surgery or biopsy were stained with the anti-G6PD antibody (1:25, HPA000247, Sigma,) and VECTASTAIN ABC-AP Kit (Vector Laboratories) to determine the presence of G6PD expression in tumor cells.

Statistical analysis

All experiments were performed in triplicate at least three separate times and the average value and SD were reported. Statistical analyses were performed by using Graph Pad Prism V.9 (Graph Pad Software, San Diego, California, USA) and Pharmaco Analyst Software (Humanlife, Tokyo, Japan). Probability values of less than 0.05 were considered statistically significant.

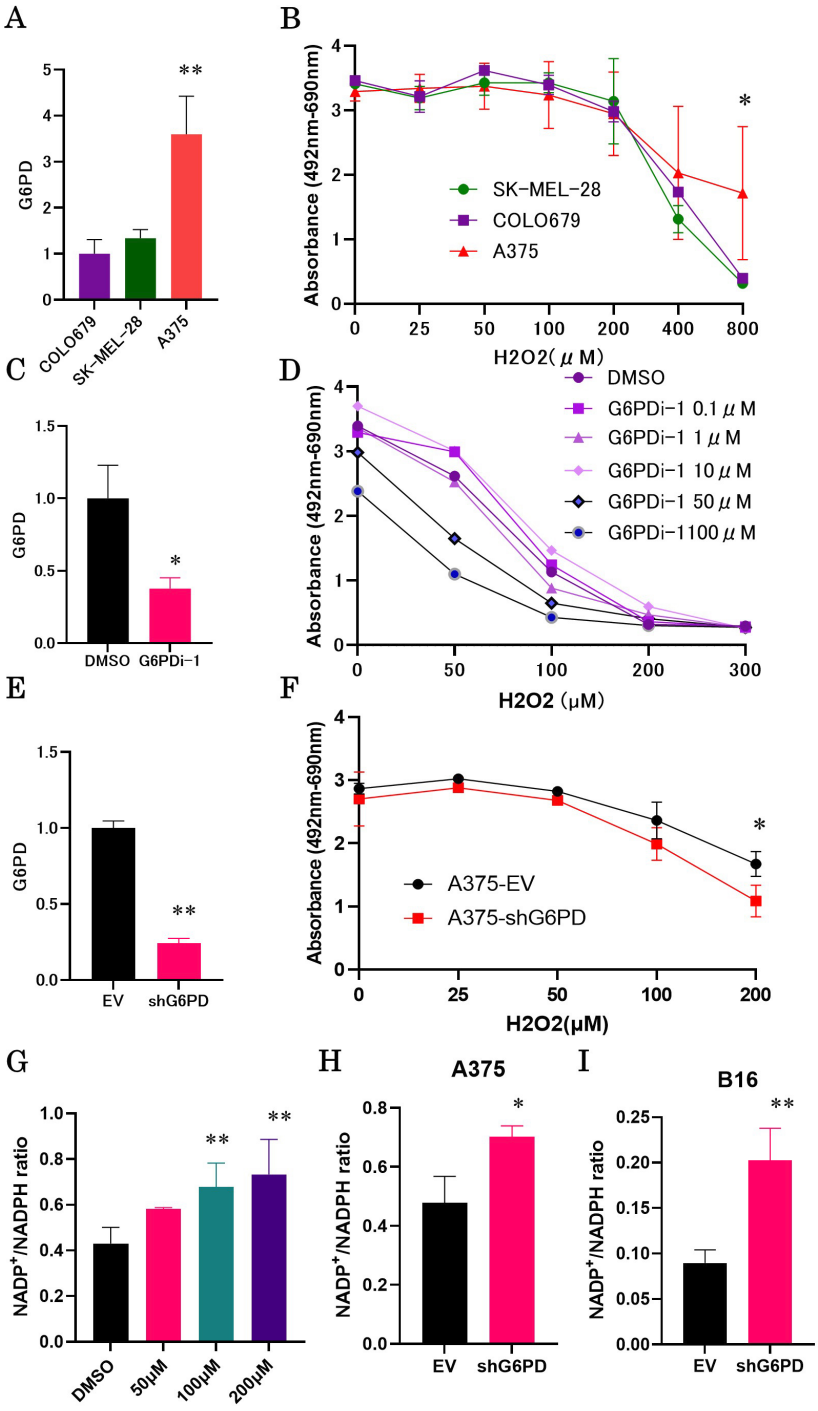

Figure 1 Glucose-6-phosphate dehydrogenase (G6PD) inhibition in melanoma cell lines. G6PD expression in each melanoma cell line was quantified by qRT-PCR. A375 melanoma cells had the highest G6PD expression compared with other cell lines (p=0.0014, Dunnett's test) (A). Each melanoma cell line was analyzed for resistance to oxidative damage in an XTT assay in a dose course of H2O2. A375 melanoma cells were significantly more resistant to oxidative damage than the other cell lines (p=0.0489, Dunnett's test) (B). G6PD in melanoma cells (COLO679) was inhibited by G6PDi-1 100 µM and decreased expression was confirmed by qRT-PCR (p=0.011, Student's t-test) (C). COLO679 melanoma cells showed decreased tolerance to H_2O_2 in a G6PDi-1 concentration-dependent manner in XTT assay (D). A375 melanoma cells genetically blocked for G6PD with shRNA also showed significantly reduced G6PD expression by qRT-PCR (p<0.00001, Student's t-test) (E). A375 melanoma cells genetically blocked for G6PD with shRNA were significantly less resistant to oxidative damage when 200 µM H2O2 was added compared with cells transfected with empty vector (p=0.0328, Student's t-test) (F). NADPH production in COLO679 melanoma cells during G6PD inhibition was measured by the NADP+/NADPH assay. The $NADP^+$/NADPH ratio was increased by the concentration of G6PDi-1 (p≤0.01, Williams' test) (G). G6PD blocked A375 human melanoma cell line had an increased the $NADP^+$/NADPH ratio (p≤0.05, Student's t-test) (H). G6PD blocked B16 mouse melanoma cell line had an increased the $NADP^+$/NADPH ratio (p≤0.01, Student's t-test) (I). Experiments were performed in biological triplicates. Error bars show±SD. *p ≤ 0.05, **p ≤ 0.01. EV, empty vector.

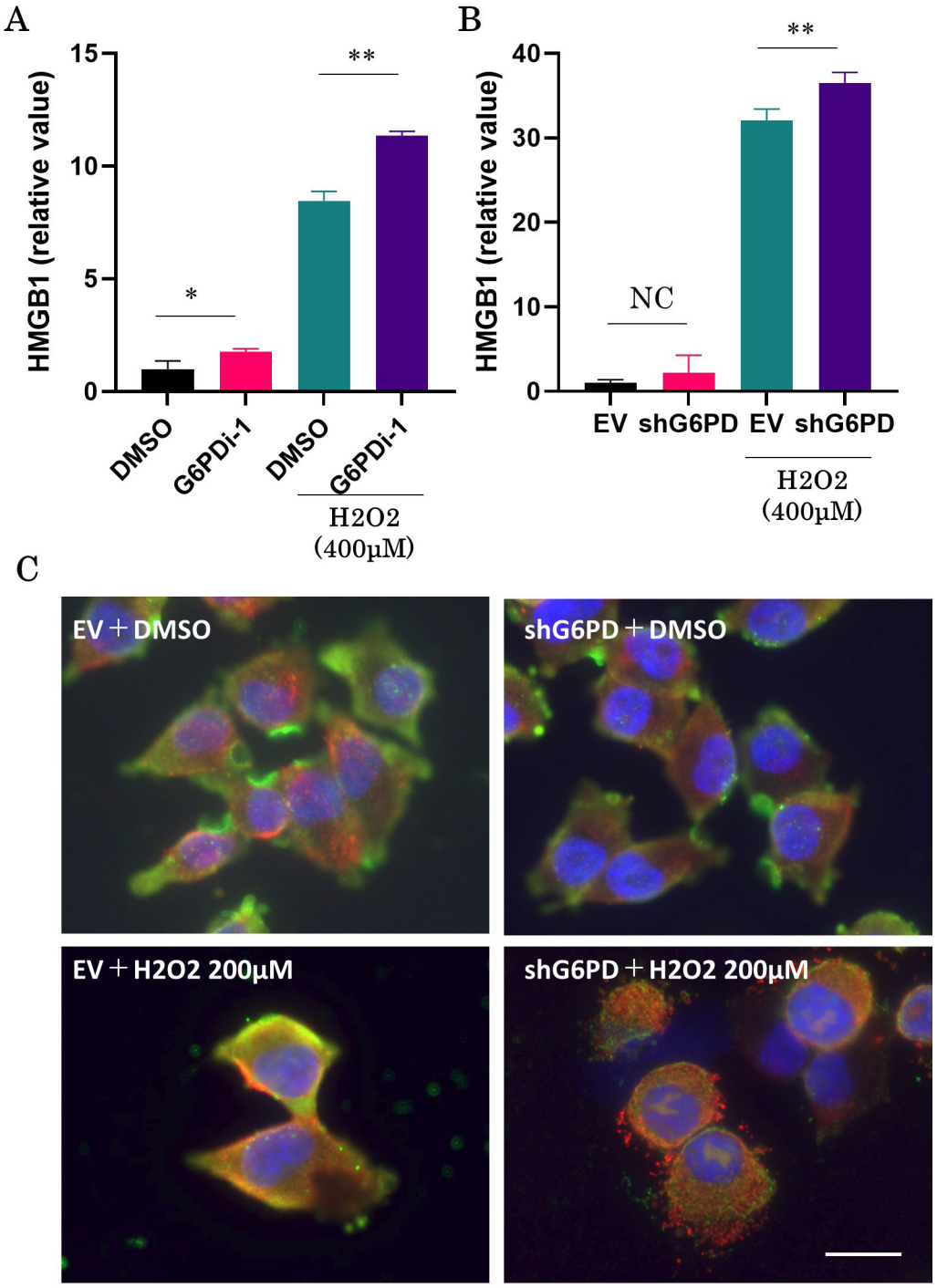

Figure 2 High mobility group box 1 (HMGB1) assay and immunofluorescent of calreticulin. HMGB1 is measured in the culture medium supernatant with or without 400 µM H_2O_2 and 100 µM G6PDi-1. HMGB1 is elevated in the culture medium of glucose-6-phosphate dehydrogenase (G6PD)-inhibited COLO679 melanoma cells (A). A375 melanoma cells in which G6PD was blocked with shRNA were also treated with 400 µM H_2O_2, and HMGB1 was measured in the culture medium supernatant 24 hours later. There is no difference in the amount of HMGB1 released without the addition of H2O2, but the addition of H2O2 increases HMGB1 release, significantly more than in melanomas transfected with empty vector (B). Immunofluorescent with calreticulin stained red, β-actin stained green, and nuclei stained blue show calreticulin migrating to the cell membrane surface in melanoma cells with 200 µM H_2O_2. Scale bar, 20 µm (C). Experiments were performed in biological triplicates. Error bars show±SD. *p ≤ 0.05, **p ≤ 0.01.

RESULTS

Inhibition of G6PD results in decreased NADPH production and resistance to oxidative damage

Three melanoma cell lines (SK-Mel28, COLO679, A375) were cultured and G6PD expression was measured by qRT-PCR. A375 melanoma cells had the highest G6PD expression compared with other cell lines (p=0.0014, Dunnett's test, figure 1A). XTT assay at 24 hours after

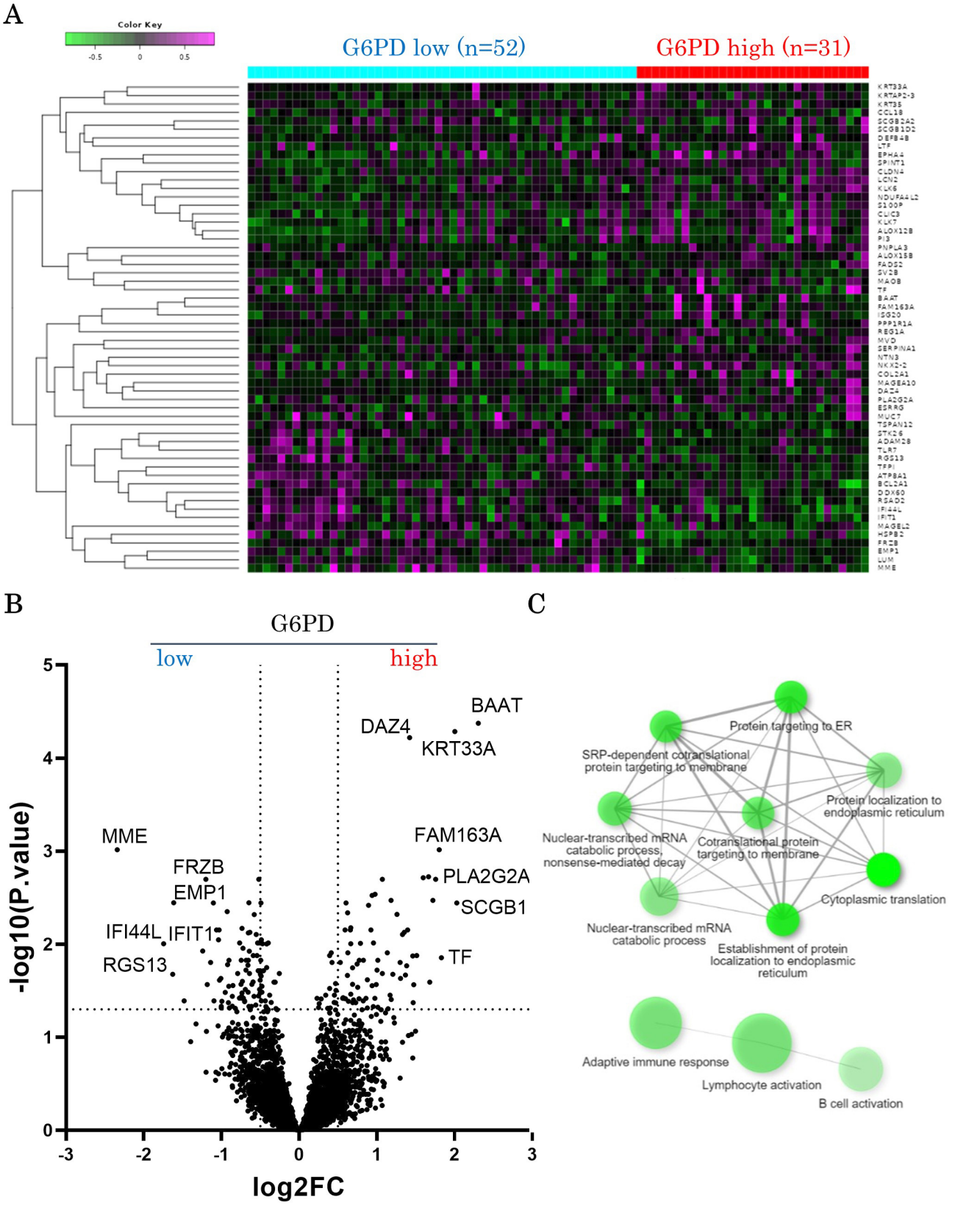

Figure 3 In silico analysis. In silico analysis was performed using the profiled data set containing 83 melanoma samples at GEO database (GSE8401). Clustering analysis reveals genes that are downregulated and upregulated in each group. Purple means high expression and green means low expression (A). Genes significantly highly expressed in each group are represented by volcano plots (B). GAGE analysis reveals sets of genes specifically upregulated in the G6PD: low group. Pathway analysis results show that 8 of the top 10 gene sets are endoplasmic reticulum target gene related, reflecting endoplasmic reticulum stress (above connecting 8 dots). Two more gene sets (7th and 8th) and the 14th gene set (B cell activation) are related to lymphocyte activation (C).

Table 1 Gene sets specifically upregulated in the low G6PD group

G6PD low	Statistic	Genes	Adjusted p value
Cytoplasmic translation	−4.8631	79	7.70E−03
Establishment of protein localization to endoplasmic reticulum	−4.4487	74	2.20E−02
Protein targeting to ER	−4.3	71	2.70E−02
SRP-dependent cotranslational protein targeting to membrane	−4.1364	67	4.00E−02
Cotranslational protein targeting to membrane	−3.9239	69	5.80E−02
Nuclear-transcribed mRNA catabolic process, nonsense-mediated decay	−3.9238	78	5.80E−02
Adaptive immune response	−3.6947	280	8.50E−02
Lymphocyte activation	−3.6503	433	8.50E−02
Protein localization to endoplasmic reticulum	−3.6352	89	1.00E−01
Nuclear-transcribed mRNA catabolic process	−3.5437	111	1.00E−01

ER, endoplasmic reticulum; G6PD, glucose-6-phosphate dehydrogenase; mRNA, messenger RNA; SRP, signal-recognition particle .

the addition of each concentration of H_2O_2 showed that A375 melanoma cells were significantly more resistant to oxidative damage than the other cell lines at 800 µM H2O2 (p=0.0489, Dunnett's test, figure 1B). G6PD in melanoma cells (COLO679) was inhibited by G6PDi-1 100 µM (p=0.011, Student's t-test, figure 1C). Melanoma cells showed decreased tolerance to H_2O_2 in a G6PDi-1 concentration-dependent manner (figure 1D). Melanoma cells genetically blocked for G6PD with shRNA also showed significantly reduced G6PD expression by qRT-PCR (p<0.00001, Student's t-test, figure 1E). Melanoma cells genetically blocked for G6PD with shRNA were significantly less resistant to oxidative damage when 200 µM H2O2 was added compared with cells transfected with empty vector (p=0.0328, Student's t-test, figure 1F). The $NADP^+$/NADPH ratio was increased by the concentration of G6PDi-1 (COLO679, Williams' test, figure 1G) and was significantly increased by knockdown of the G6PD gene (A375, figure 1H; B16 mouse melanoma, figure 1I).

Cell death by G6PD inhibition is accompanied by the release of HMGB1 and translocation of calreticulin to the cell membrane surface

400 µM H_2O_2 was added to melanoma cells in which G6PD was inhibited by 100 µM G6PDi-1. After 24 hours, only the culture medium supernatant was collected and the amount of HMGB1 protein was measured. Even without H_2O_2, HMGB1 was elevated in the culture medium of G6PD-inhibited melanoma cells but was more significantly elevated when 400 µM H2O2 was added to G6PD-inhibited melanoma cells (figure 2A). Melanoma cells in which G6PD was blocked with shRNA were also treated with 400 µM H_2O_2, and HMGB1 was measured in the culture medium supernatant 24 hours later. There was no difference in the amount of HMGB1 released without the addition of H_2O_2, but the addition of H_2O_2 increased HMGB1 release, significantly more than in melanomas transfected with empty vector (figure 2B). Immunofluorescent with calreticulin stained red, β-actin stained green, and nuclei stained blue showed calreticulin migrating to the cell membrane surface in melanoma cells with 200 µM H_2O_2 (figure 2C).

Melanoma with low G6PD expression significantly expresses gene sets associated with lymphocyte activation and endoplasmic reticulum stress

The analysis was performed using the profiled data set containing 83 melanoma samples containing 31 primary and 52 metastatic lesions with comprehensive gene expression analysis for 13,488 genes accessible at GEO database (GSE8401). Samples with *G6PD* expression higher than the average of all samples were designated high G6PD, and samples with *G6PD* expression lower than the average were designated low G6PD. 83 melanoma samples were classified into 31 samples in the high G6PD group and 52 samples in the low G6PD group. Clustering analysis revealed genes that are downregulated and upregulated in each group (figure 3A). Genes significantly highly expressed in each group were represented by volcano plots (figure 3B). For *BAAT*, *DAZ4*, and *KRT33A*, which are significantly upregulated in high G6PD group, their role in cancer is not clear. *FAM163A* is a positive regulator of the ERK signaling pathway and is associated with neuroblastoma and lung squamous cell carcinoma.[24] *PLA2G2A* is associated with esophageal adenocarcinoma and glioblastoma and has been reported to promote fatty acid synthesis and energy metabolism in pancreatic cancer cells with K-ras mutations.[25] *SCGB1D2* mutations have been reported in breast and gynecological cancers and are associated with poor prognosis in pancreatic ductal adenocarcinoma.[26] GAGE analysis revealed sets of genes specifically upregulated in the low G6PD group (table 1). Pathway analysis results showed that eight of the top 10

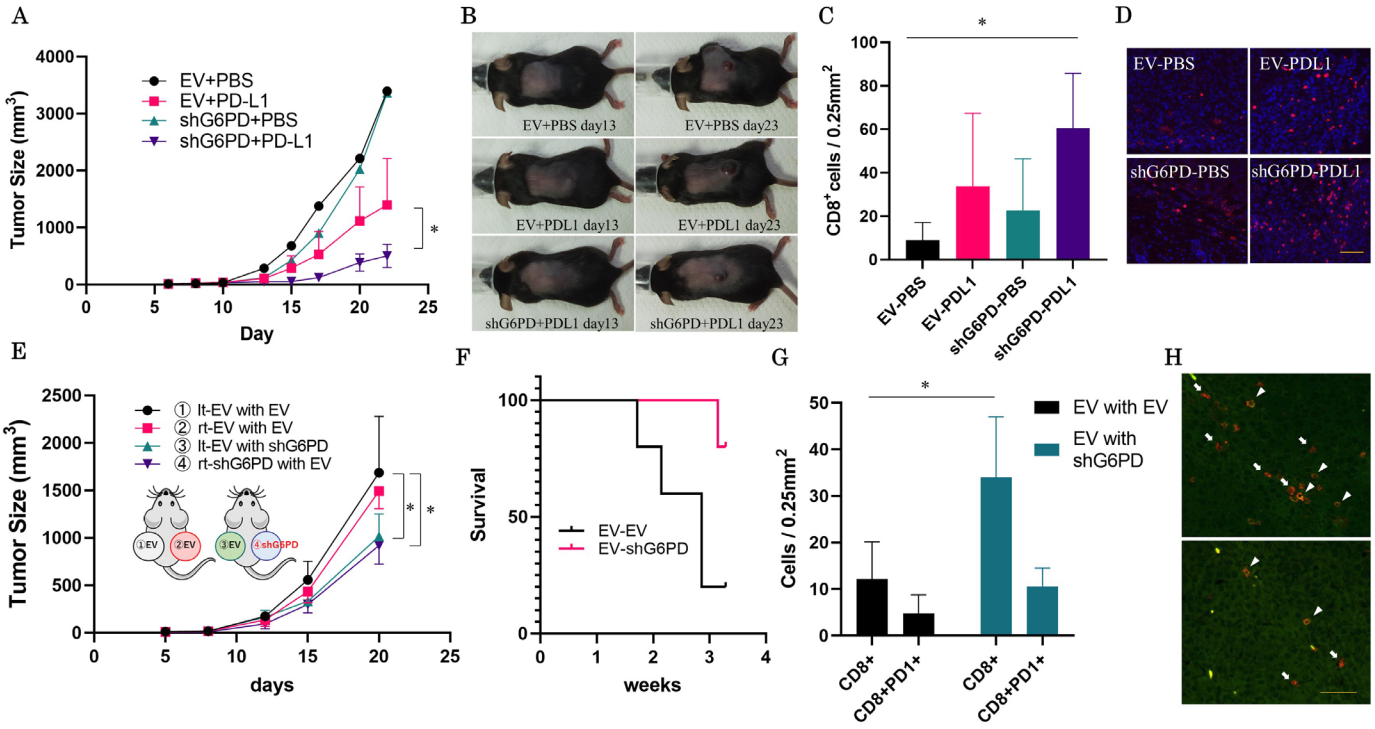

Figure 4 Glucose-6-phosphate dehydrogenase (G6PD) inhibition in melanoma mouse model. B16 melanoma cells knocked down G6PD using shRNA plasmid were injected subcutaneously into the back of C57BL/6 mice. Mice injected with B16 melanoma cells transfected with the empty vector (EV) as controls. Experiments were conducted with six mice in each of four groups. Mice treated with anti-PD-L1 antibody had smaller tumor growth than mice injected with PBS. Among those treated with twice-weekly 200 µg/mouse anti-PD-L1 antibody, mice injected with B16 knockdown of G6PD (shG6PD) show significantly smaller tumors than those injected with B16 with the empty vector (p=0.0497, Student's t-test) (A). Examples of representative mice are shown (B). Fluorescent immunostaining counts of the number of infiltrating CD8-positive cells using tumors obtained on day 23 showed that shG6PD melanomas treated with anti-PD-L1 had significantly more cellular infiltration than other tumors (p=0.027, Tukey test) (C). Representative images of immunofluorescent staining for CD8 (red) (D). Mice were injected subcutaneously with B16 melanoma cells at two sites on either side of the back. One group was injected subcutaneously with EV-transfected tumor on both the left and right sides, and the other group was injected subcutaneously with EV-transfected tumor on the left and a G6PD shRNA-blocked tumor on the right. Both groups were treated with 200 µg/mouse anti-PD-L1 antibody twice a week. Experiments were conducted with five mice in each of two groups. Comparing tumor size after 20 days, not only the shG6PD tumor (p=0.0186, Dunnett's test) but also the EV-transfected tumors of mice with shG6PD tumors (p=0.0393, Dunnett's test), significantly inhibited tumor growth compared with mice without blocked G6PD was observed (E). There was a significant difference in survival between the group that blocked G6PD in some tumors and the group that did not. (p=0.0357, log-rank test) (F). Immunohistochemistry comparison of the number of lymphocytes infiltrating EV-transfected tumors on the left back of mice in each group showed that CD8-positive cells were significantly increased in mice with G6PD knockdown tumors on the right back (p=0.0128, Student's t-test) (G). Representative images of immunofluorescent staining for CD8 (red) and PD1 (green). Arrows point to CD8 alone positive cells, and arrowheads point to double-positive cells for CD8 and PD1. Scale bar, 50 µm (H). All mouse experiments were repeated three times with essentially similar results. *p ≤ 0.05.

gene sets were endoplasmic reticulum target gene related, reflecting endoplasmic reticulum stress. Two more gene sets (7th and 8th) and the 14th gene set (B cell activation, not shown in table 1) were related to lymphocyte activation (figure 3C).

Mice seeded with G6PD knockdown tumors responded well to ICIs

Mice treated with anti-PD-L1 antibody had smaller tumor growth than mice injected with PBS. Among those treated with anti-PD-L1 antibody, Mice injected with B16 knockdown of G6PD showed significantly smaller tumors than those injected with B16 with the empty vector (p=0.0497, Student's t-test, figure 4A,B). Tumors in mice injected with PBS but not anti-PD-L1 antibody showed no difference between G6PD knockdown melanoma cells and empty vector controls. It can be said that mice seeded with tumors in which G6PD was knocked down responded well to ICIs. Fluorescent immunostaining counts of the number of infiltrating CD8-positive cells using tumors obtained on day 23 showed that G6PD knockdown melanomas treated with PD-L1 had significantly more cellular infiltration than other tumors (p=0.027, Tukey test, figure 4C,D).

Inhibition of G6PD in a part of the tumor enhances the efficacy of immunotherapy for tumors at other sites

Mice were injected subcutaneously with B16 melanoma cells at two sites on either side of the back. One group was injected subcutaneously with an empty vector

(EV)-transfected tumor on both the left and right sides, and the other group was injected subcutaneously with EV-transfected tumor on the left and a G6PD shRNA-knocked down tumor on the right. Both groups were treated with 200 µg/mouse anti-PD-L1 antibody twice a week. Comparing tumor size after 20 days, not only the shG6PD tumor (p=0.0186, Dunnett's test) but also EV-transfected tumors of mice with shG6PD tumors, significantly inhibited tumor growth compared with mice without knocked down G6PD was observed (p=0.0393, Dunnett's test, figure 4E). In addition, significant differences in mouse survival were also observed (p=0.0357, log-rank test, figure 4F). Quantitative comparison of immunohistochemical staining of lymphocytes infiltrating EV-transfected tumors on the left back of mice in each group revealed that the number of CD8-positive cells was significantly higher in mice with G6PD knockdown tumors on the right back (p=0.0128, Student's t-test), which correlated with tumor shrinkage. While the number of CD8 and PD1 double-positive cells was also increased, the ratio of PD1-positive cells to total CD8-positive cells was unchanged (figure 4G,H).

G6PD-negative melanoma and lung cancer patients treated with ICI had prolonged progression-free survival compared with G6PD-positive patients

We analyzed 42 patients with pathologically diagnosed cutaneous malignant melanoma who were treated with ICIs at Nagoya City University Hospital. The cohort included 26 men and 16 women with a median age of 70. They were one-third low CSD, one-third Acral type, followed by Mucosal and High CSD. Three cases were primary unknown. They were treated with nivolumab, pembrolizumab, or nivolumab+ipilimumab combination therapy (table 2). The G6PD negative group showed longer progression-free survival (PFS) than the positive group (p=0.0473, log-rank test, figure 5A). G6PD positivity or negativity was determined by immunostaining. If more than 10% of tumor cells stained red, they were considered positive. If less than 10%, they were considered negative. The cases were clearly distinguishable, as in the representative case (figure 5B). There was no significant difference in the occurrence of grade III or higher immune-related adverse events (irAE) in each group (Fisher's exact test, figure 5C).

The lung cancer cohort consisted of 30 patients, 26 males and 4 females, with a mean age of 68.8. adenocarcinoma accounted for 73.3% of the cases. Treatment consisted of nivolumab, pembrolizumab, atezolizumab, durvalumab,

Table 2 Characteristics of melanoma patients and lung cancer patients

Characteristics	Melanoma		Lung cancer	
Cases		42		30
Age (range)		70.55 (40–86)		68.80 (44–87)
Sex				
Male		26 (61.9%)		26 (86.7%)
Female		16 (38.1%)		4 (13.3%)
Race				
Asian (Japanese)		61 (100%)		30 (100%)
Type				
	Low CSD	14 (33.3%)	Adeno	22 (73.3%)
	High CSD	5 (11.9%)	Squamous	4 (13.3%)
	Acral	14 (33.3%)	Small cell	3 (10.0%)
	Mucosal	6 (14.3%)	LCNEC	1 (3.3%)
	Primary unknown	3 (7.1%)		
ICI				
	Nivolumab	20 (47.6%)	Nivolumab	7 (23.3%)
	Pembrolizumab	12 (28.6%)	Pembrolizumab	18 (60.0%)
	Nivo+Ipi	10 (23.8%)	Atezolizumab	1 (3.3%)
			Durvalumab	1 (3.3%)
			Pembro+CBDCA+PEM	2 (6.7%)
			Nivo+Ipi	1 (3.3%)

Total percentage values might sum to <100% due to rounding.
CBDCA, carboplatin; CSD, cumulative sun damage; ICI, immune checkpoint inhibitor; Ipi, Ipilimumab; LCNEC, large cell neuroendocrine carcinoma; Nivo, nivolumab; PEM, pemetrexed; Pembro, pembrolizumab;

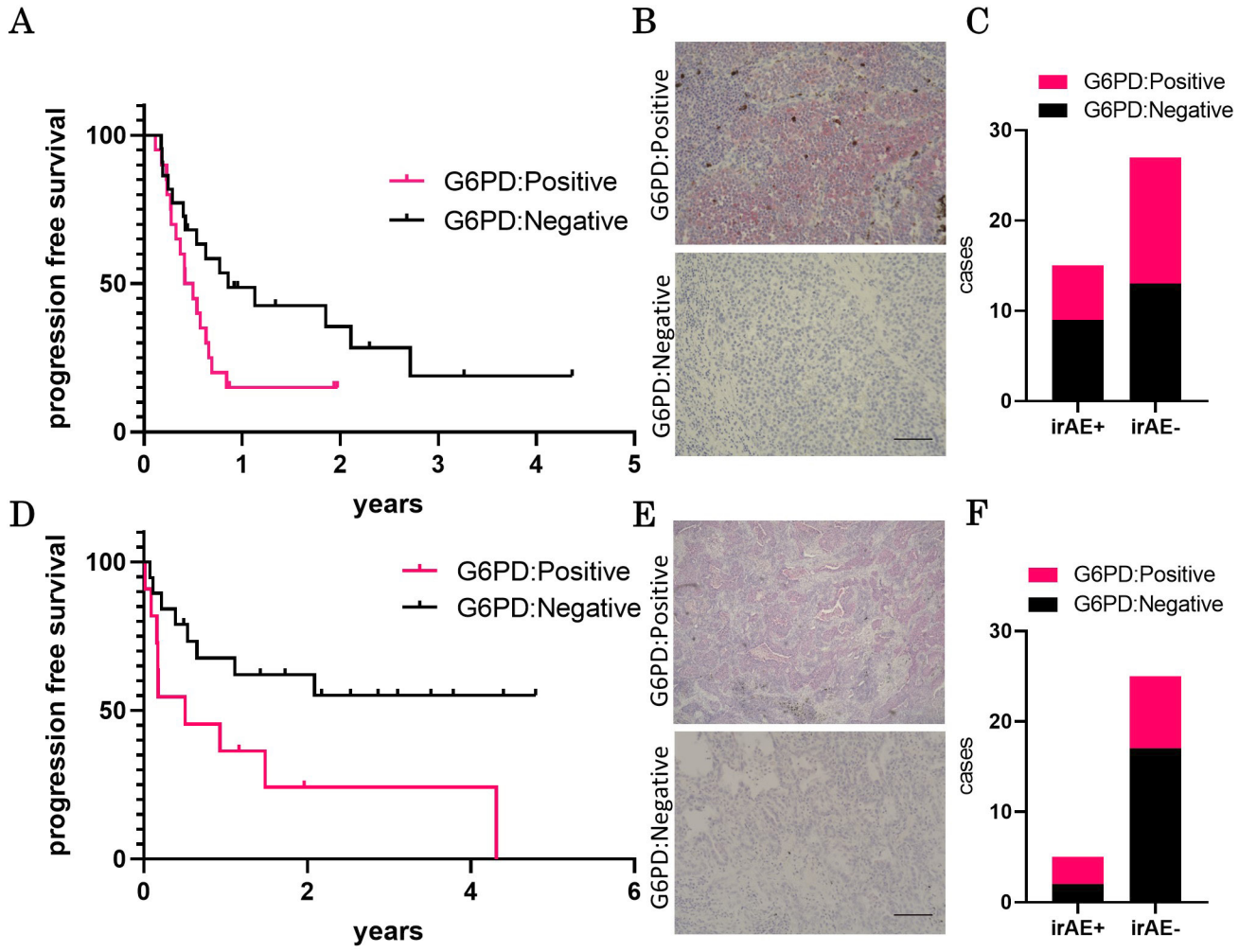

Figure 5 Cohort study of melanoma and lung cancer patients. The Glucose-6-phosphate dehydrogenase (G6PD) negative melanoma (n=22) showed longer progression-free survival than the positive melanoma (n=20) (p=0.0473, log-rank test) (A). Representative images of G6PD positive and negative melanoma samples. Scale bar, 100 µm (B). There was no significant difference in the occurrence of grade III or higher irAE in each group (Fisher's exact test) (C). The G6PD negative lung cancer (n=19) showed longer progression-free survival than the positive lung cancer (n=11) (p=0.0287, log-rank test) (D). Representative images of G6PD positive and negative lung cancer samples. Scale bar, 100 µm (E). There was no significant difference in the occurrence of grade III or higher irAE in each group (Fisher's exact test) (F).

pembrolizumab+carboplatin (CBDCA)+pemetrexed (PEM), or nivolumab+ipilimumab combination therapy (table 2). Also in this cohort, the G6PD negative group showed longer PFS than the positive group (p=0.0287, log-rank test, figure 5D). The presence or absence of G6PD expression was determined by the same method as for melanoma. Representative cases were shown (figure 5E). There was no significant difference in the occurrence of grade III or higher irAE in each group (Fisher's exact test, figure 5F).

DISCUSSION

According to this study, inhibiting G6PD reduces NADPH production and causes ICD in tumor cells, making them more vulnerable to oxidative damage. This ICD activates the tumor immunity and strengthens the effects of ICIs. The study shows that the expression of G6PD is inversely related to the effectiveness of ICIs in melanoma and lung cancer. These cancers have a higher tumor mutation burden and are more sensitive to the activation of tumor immunity by suppressing G6PD expression. This research is the first to reveal the mechanism of tumor immune activation by G6PD inhibition, which is beneficial for the provision of more effective immunotherapy. It strongly supports the clinical application of G6PD inhibition in cancer therapy.

Since PPP is the major glucose metabolic pathway in cancer cells, inhibition of G6PD could be a promising strategy in cancer therapy. As already mentioned, G6PD deficiency is a genetic disorder that is seen with some frequency and its relationship to cancer development has been investigated. A 17-year, 11708-person study at a teaching hospital in Northern Sardinia, Italy, found that G6PD deficiency lowers the risk of gastric, hepatocellular, and[27] colorectal cancer.[28 29] The less of cancer susceptibility in G6PD deficiency raises hopes for the application of G6PD inhibition to anticancer therapy.

There have been several reports of previous efforts to treat cancer by inhibiting G6PD.[8] 6-Aminonicotinamide (6-AN) is a well-known competitive inhibitor of G6PD that is structurally similar to NADP.[30] It has been demonstrated radiosensitizing activity against malignant tumors in combination with 2-deoxy-D-glucose[15 31 32] and antitumor effects against breast and bladder cancer in combination with cisplatin or 5-fluorouracil.[33 34] However, it is a competitive inhibitor with limited efficacy and is not suitable for real-world clinical use due to the complications of severe neurological deficits.[35] Dehydroepiandrosterone (DHEA) is a type of adrenal steroid that is a noncompetitive inhibitor of G6PD. It has been reported to have anticancer activity against cervical cancer cells,[36] but clinical application is still far from practical because high doses must be taken internally and DHEA must be converted to other active forms.[12]

As a new G6PD inhibitor in 2018, Polydatin (3,4′,5 -trihydroxystilbene-3-β-d-glucoside; trans-resveratrol 3-β-mono-D-glucoside; piceid), a natural molecule found in the tapeworm and other plants, was reported.[37] Polydatin induces cell death due to ER stress and oxidative damage via inhibition of G6PD, inhibiting oral cancer cell proliferation and lymph node metastasis. Polydatin has been administered in various animal models at doses up to 200 mg/kg and no significant cardiovascular, liver, bone marrow, or renal toxicity has been reported.[38–40] In humans, phase II clinical trials for other non-cancer diseases (irritable bowel syndrome, endometriosis-related pain) have been conducted using doses ranging from 20 to 40 mg twice daily for up to 3 months with no significant toxic effects reported.[41 42] Polydatin, like other G6PD inhibitors, has also been reported to have synergistic effects when used in combination with cisplatin and other drugs.[37] However, the relationship between these G6PD inhibitors and tumor immunity and their efficacy in combination with immunotherapy has not been investigated to date.

Closer to clinical application, zoledronic acid (ZA), the current standard of treatment for patients with bone metastases or osteoporosis, was reported to inhibit G6PD.[43] ZA inhibits TAp73 stability and reduces G6PD activity via blockade of Ras signaling. ZA has a direct effect on tumor cells as well as on bone metastases.[44 45] Like other G6PD inhibitors, it has also been reported to be effective in combination with cytotoxic anticancer agents.[46] In 2022, ZA was tested in combination with anti-PD-1 antibody, an ICI, for non-small cell lung cancer and showed significantly longer PFS (HR: 0.520, p=0.028,) and higher disease control rates (75.0% vs 51.7%, p=0.049) than anti-PD-1 antibody therapy alone.[47] Although the association with G6PD inhibition was not examined, interestingly, an enhancement of antitumor immunity was observed in the combination group, with more CD8+IFN-γ+T cells and γδ T cells in the circulation and tumor-infiltrating lymphocytes. G6PD inhibition and ICD induction by ZA may be one of the mechanisms for its antitumor immune activation.

G6PD inhibition can induce ICD, which can be beneficial for cancer therapy. However, to achieve the full effect of ICD induction, G6PD inhibition should be combined with immunotherapy. The current study also suggests a new form of clinical application where the local injection of G6PD inhibitors into skin metastases or lymph nodes can enhance the effect of ICIs. This is similar to the abscopal effect of radiotherapy. Furthermore, the observation that G6PD inhibition of a part of the tumor also inhibited the growth of other tumors via enhancement of antitumor immunity is significant. The present study's findings reveal the potential of G6PD inhibition in cancer therapy, which has been investigated in various ways.

Acknowledgements This work was supported by the 5th Takagi award from Maruho Takagi Dermatology Foundation, the 15th Rohto award from Japanese Association of Geriatric Dermatology Research, and the Hori Sciences and Arts Foundation. We thank Ms Kasuya and Ms Nishioka for their technical assistance.

Contributors MN and AM conceived and designed the study. MN acquired data sets, analyzed the data and wrote the manuscript. MN, TM, and MY carried out the experimental work. MN, MY, SK, HK, KY, and KO collected samples. KO and AM revised the manuscript. All authors read and approved the final manuscript. MN is responsible for the overall content as the guarantor.

Funding This work was supported by the 5th Takagi award from Maruho Takagi Dermatology Foundation, the 15th Rohto award from Japanese Association of Geriatric Dermatology Research, and the Hori Sciences and Arts Foundation.

Competing interests Nagoya City University is submitting patents for the G6PD test methods. MN invented the G6PD test method.

Patient consent for publication Not applicable.

Ethics approval This study involves human participants and was approved by Nagoya City University Clinical Trial Management Center, No. 60-22-0141. Participants gave informed consent to participate in the study before taking part.

Provenance and peer review Not commissioned; externally peer reviewed.

Data availability statement Data are available on reasonable request. The data underlying this article will be shared on reasonable request to the corresponding author.

ORCID iD

Motoki Nakamura http://orcid.org/0000-0003-4431-7782

REFERENCES

1 Nakamura M, Nagase K, Yoshimitsu M, *et al*. Glucose-6-phosphate dehydrogenase correlates with tumor immune activity and programmed death ligand-1 expression in merkel cell carcinoma. *J Immunother Cancer* 2020;8:e001679.
2 Stanton RC. Glucose-6-phosphate dehydrogenase, NADPH, and cell survival. *IUBMB Life* 2012;64:362–9.
3 Luzzatto L, Arese P. Favism and glucose-6-phosphate dehydrogenase deficiency. *N Engl J Med* 2018;378:60–71.
4 WARBURG O. On the origin of cancer cells. *Science* 1956;123:309–14.
5 Gatenby RA, Gillies RJ. Why do cancers have high aerobic glycolysis? *Nat Rev Cancer* 2004;4:891–9.
6 Kim J, Dang CV. Cancer's molecular sweet tooth and the Warburg effect. *Cancer Res* 2006;66:8927–30.
7 Vander Heiden MG, Cantley LC, Thompson CB. Understanding the warburg effect: the metabolic requirements of cell proliferation. *Science* 2009;324:1029–33.
8 Yang H-C, Wu Y-H, Yen W-C, *et al*. The redox role of G6PD in cell growth, cell death, and cancer. *Cells* 2019;8:1055.

9 Hu T, Zhang C, Tang Q, *et al*. Variant G6PD levels promote tumor cell proliferation or apoptosis via the STAT3/5 pathway in the human melanoma xenograft mouse model. *BMC Cancer* 2013;13:251.
10 Vizán P, Alcarraz-Vizán G, Díaz-Moralli S, *et al*. Modulation of pentose phosphate pathway during cell cycle progression in human colon adenocarcinoma cell line HT29. *Int J Cancer* 2009;124:2789–96.
11 Lu M, Lu L, Dong Q, *et al*. Elevated G6PD expression contributes to migration and invasion of hepatocellular carcinoma cells by inducing epithelial-mesenchymal transition. *Acta Biochim Biophys Sin (Shanghai)* 2018;50:370–80.
12 Zhang C, Zhang Z, Zhu Y, *et al*. Glucose-6-phosphate dehydrogenase: a biomarker and potential therapeutic target for cancer. *Anticancer Agents Med Chem* 2014;14:280–9.
13 Leopold JA, Walker J, Scribner AW, *et al*. Glucose-6-phosphate dehydrogenase modulates vascular endothelial growth factor-mediated angiogenesis. *J Biol Chem* 2003;278:32100–6.
14 Yang X, Ye H, He M, *et al*. LncRNA PDIA3P interacts with c-Myc to regulate cell proliferation via induction of pentose phosphate pathway in multiple myeloma. *Biochem Biophys Res Commun* 2018;498:207–13.
15 Sharma PK, Bhardwaj R, Dwarakanath BS, *et al*. Metabolic oxidative stress induced by a combination of 2-DG and 6-AN enhances radiation damage selectively in malignant cells via non-coordinated expression of antioxidant enzymes. *Cancer Lett* 2010;295:154–66.
16 Zhang R, Tao F, Ruan S, *et al*. The TGFβ1-FOXM1-HMGA1-TGFβ1 positive feedback loop increases the cisplatin resistance of non-small cell lung cancer by inducing G6PD expression. *Am J Transl Res* 2019;11:6860–76.
17 Sharma N, Bhushan A, He J, *et al*. Metabolic plasticity imparts erlotinib-resistance in pancreatic cancer by upregulating glucose-6-phosphate dehydrogenase. *Cancer Metab* 2020;8:19.
18 Polimeni M, Voena C, Kopecka J, *et al*. Modulation of doxorubicin resistance by the glucose-6-phosphate dehydrogenase activity. *Biochem J* 2011;439:141–9.
19 Pu H, Zhang Q, Zhao C, *et al*. Overexpression of G6PD is associated with high risks of recurrent metastasis and poor progression-free survival in primary breast carcinoma. *World J Surg Oncol* 2015;13:323.
20 Tang Y-C, Hsiao J-R, Jiang S-S, *et al*. c-MYC-directed NRF2 drives malignant progression of head and neck cancer via glucose-6-phosphate dehydrogenase and transketolase activation. *Theranostics* 2021;11:5232–47.
21 Wang J, Yuan W, Chen Z, *et al*. Overexpression of G6PD is associated with poor clinical outcome in gastric cancer. *Tumour Biol* 2012;33:95–101.
22 Xu L, Shen SS, Hoshida Y, *et al*. Gene expression changes in an animal melanoma model correlate with aggressiveness of human melanoma metastases. *Mol Cancer Res* 2008;6:760–9.
23 Ge SX, Son EW, Yao R. IDEP: an integrated web application for differential expression and pathway analysis of RNA-seq data. *BMC Bioinformatics* 2018;19:534.
24 Liu N, Zhou H, Zhang X, *et al*. FAM163A, a positive regulator of ERK signaling pathway, interacts with 14-3-3β and promotes cell proliferation in squamous cell lung carcinoma. *Onco Targets Ther* 2019;12:6393–406.
25 Zhang M, Xiang R, Glorieux C, *et al*. PLA2G2A phospholipase promotes fatty acid synthesis and energy metabolism in pancreatic cancer cells with K-ras mutation. *IJMS* 2022;23:11721.
26 Liu W, Fu X-L, Yang J-Y, *et al*. Elevated expression of CTHRC1 predicts unfavorable prognosis in patients with pancreatic ductal adenocarcinoma. *Am J Cancer Res* 2016;6:1820–7.
27 Büttner R, Longshore JW, López-Ríos F, *et al*. Implementing TMB measurement in clinical practice: considerations on assay requirements. *ESMO Open* 2019;4:e000442.
28 Pes GM, Errigo A, Soro S, *et al*. Glucose-6-phosphate dehydrogenase deficiency reduces susceptibility to cancer of endodermal origin. *Acta Oncol* 2019;58:1205–11.
29 Pes GM, Bassotti G, Dore MP. Colorectal cancer mortality in relation to glucose - 6 - phosphate dehydrogenase deficiency and consanguinity in Sardinia: a spatial correlation analysis. *Asian Pac J Cancer Prev* 2017;18:2403–7.
30 Köhler E, Barrach H-J, Neubert D. Inhibition of NADP dependent oxidoreductases by the 6-aminonicotinamide analogue of NADP. *FEBS Lett* 1970;6:225–8.
31 Sharma PK, Varshney R. 2-deoxy-D-glucose and 6-aminonicotinamide-mediated Nrf2 down regulation leads to radiosensitization of malignant cells via abrogation of GSH-mediated defense. *Free Radic Res* 2012;46:1446–57.
32 Varshney R, Gupta S, Dwarakanath BS. Radiosensitization of murine Ehrlich ascites tumor by a combination of 2-deoxy-D-glucose and 6-aminonicotinamide. *Technol Cancer Res Treat* 2004;3:659–63.
33 Stolfi RL, Colofiore JR, Nord LD, *et al*. Biochemical modulation of tumor cell energy: regression of advanced spontaneous murine breast tumors with a 5-fluorouracil-containing drug combination. *Cancer Res* 1992;52:4074–81.
34 Chen X, Xu Z, Zhu Z, *et al*. Modulation of G6PD affects bladder cancer via ROS accumulation and the AKT pathway in vitro. *Int J Oncol* 2018;53:1703–12.
35 Gupte SA. Glucose-6-phosphate dehydrogenase: a novel therapeutic target in cardiovascular diseases. *Curr Opin Investig Drugs* 2008;9:993–1000.
36 Fang Z, Jiang C, Feng Y, *et al*. Effects of G6PD activity inhibition on the viability, ROS generation and mechanical properties of cervical cancer cells. *Biochim Biophys Acta* 2016;1863:2245–54.
37 Mele L, Paino F, Papaccio F, *et al*. A new inhibitor of glucose-6-phosphate dehydrogenase blocks pentose phosphate pathway and suppresses malignant proliferation and metastasis in vivo. *Cell Death Dis* 2018;9:572.
38 Du J, Sun L-N, Xing W-W, *et al*. Lipid-lowering effects of polydatin from polygonum cuspidatum in hyperlipidemic hamsters. *Phytomedicine* 2009;16:652–8.
39 Xing WW, Wu JZ, Jia M, *et al*. Effects of polydatin from polygonum cuspidatum on lipid profile in hyperlipidemic rabbits. *Biomed Pharmacother* 2009;63:457–62.
40 Wang H-L, Gao J-P, Han Y-L, *et al*. Comparative studies of polydatin and resveratrol on mutual transformation and antioxidative effect in vivo. *Phytomedicine* 2015;22:553–9.
41 Cremon C, Stanghellini V, Barbaro MR, *et al*. Randomised clinical trial: the analgesic properties of dietary supplementation with palmitoylethanolamide and polydatin in irritable bowel syndrome. *Aliment Pharmacol Ther* 2017;45:909–22.
42 Indraccolo U, Indraccolo SR, Mignini F. Micronized palmitoylethanolamide/trans-polydatin treatment of endometriosis-related pain: a meta-analysis. *Ann Ist Super Sanita* 2017;53:125–34.
43 Wang X, Wu G, Cao G, *et al*. Zoledronic acid inhibits the pentose phosphate pathway through attenuating the Ras-TAp73-G6PD axis in bladder cancer cells. *Mol Med Rep* 2015;12:4620–5.
44 Van Acker HH, Anguille S, Willemen Y, *et al*. Bisphosphonates for cancer treatment: mechanisms of action and lessons from clinical trials. *Pharmacol Ther* 2016;158:24–40.
45 Muinelo-Romay L, Garcia D, Alonso-Alconada L, *et al*. Zoledronic acid as an antimetastatic agent for different human tumor cell lines. *Anticancer Res* 2013;33:5295–300.
46 Ottewell PD, Brown HK, Jones M, *et al*. Combination therapy inhibits development and progression of mammary tumours in immunocompetent mice. *Breast Cancer Res Treat* 2012;133:523–36.
47 Zheng Y, Wang P, Fu Y, *et al*. Zoledronic acid enhances the efficacy of immunotherapy in non-small cell lung cancer. *Int Immunopharmacol* 2022;110:109030.